International Journal of Computational Methods
Vol. 11, No. 3 (2014) 1343002 (25 pages)

DOI: 10.1142/S0219876213430020

World Scientific
www.worldscientific.com

MECHANICAL CHARACTERIZATION OF MATERIALS AND DIAGNOSIS OF STRUCTURES BY INVERSE ANALYSES: SOME INNOVATIVE PROCEDURES AND APPLICATIONS

GIULIO MAIER*

Department of Structural Engineering
Politecnico di Milano, Piazza Leonardo da Vinci 32
Milano 20133, Italy
giulio.maier@polimi.it

VLADIMIR BULJAK

Faculty of Mechanical Engineering
University of Belgrade, 80 Kraljice Marije Str.
Belgrade 11000, Serbia
vbuljak@mas.bg.ac.rs

TOMASZ GARBOWSKI

Institute of Structural Engineering
Poznan University of Technology, ul. Piotrowo 5
Poznan 60-965, Poland
tomasz.garbowski@put.poznan.pl

GIUSEPPE COCCHETTI† and GIORGIO NOVATI‡

Department of Structural Engineering
Politecnico di Milano, Piazza Leonardo da Vinci 32
Milano 20133, Italy
†*giuseppe.cocchetti@polimi.it*
‡*giorgio.novati@polimi.it*

Received 12 March 2012
Accepted 3 July 2012
Published 16 October 2013

A survey is presented herein of some recent research contributions to the methodology of inverse structural analysis based on statical tests for diagnosis of possibly damaged structures and for mechanical characterization of materials in diverse industrial environments. The following issues are briefly considered: identifications of parameters in material models and of residual stresses on the basis of indentation experiments; mechanical characterization of free-foils and laminates by cruciform and compression tests and

*Corresponding author.

digital image correlation measurements; diagnosis, both superficially and in depth, of concrete dams, possibly affected by alkali-silica-reaction or otherwise damaged.

Keywords: Inverse analysis; parameter identification; digital image correlation; proper orthogonal decomposition; trust region algorithm; artificial neural networks.

1. Introduction

Methods for accurate simulations of the behavior of engineering structures have been developed very significantly in theoretical, computational and experimental mechanics during the last decades. Powerful computational tools are now available for structural design or safety margin assessments in engineering practice. Crucial in many practical situations is the reliable estimation of parameters to be input into these computational tools in order to make realistic and accurate the results of structural analyses (see e.g., [Bui (1994, 2006)]). Such estimation can be based at present on suitably designed experiments and inverse analyses, closely related to each other in a synergistic way in order to ensure accuracy of parameter estimation and also to reduce computing times and costs.

In the above context the main methodological issues briefly presented by examples herein can be listed as follows: sensitivity analyses for the selection, in terms of both quality and quantity, of experimental data to exploit in the inverse problem in order to make it well posed; minimization of the discrepancy between measured and computed quantities by a deterministic approach; search for the absolute minimum of the discrepancy function made economical and fast by preliminary once-for-all computations (proper orthogonal decomposition); adjustments of experimental equipment and procedure in view of inverse analysis methodological requirements.

Focused are here recent results achieved by a research team at the Technical University (Politecnico) of Milan and by visiting co-workers (co-authors of here referenced publications). Several meaningful contributions provided by other teams to this growing area of engineering mechanics are not considered for brevity in this lecture. As further limitations the present survey does not cover inverse problems based on dynamical external actions, nor stochastic parameter identification procedures, such as Kalman filters.

2. Main Methodological Features

Meaningful practical advantages emerge in several technologies if structural diagnosis and material characterizations can be performed in a nondestructive fashion, possibly "*in situ*" without service interruptions, repeatedly by fast and economical procedures (economical both as for computer hardware demand and as for professional level of the operators). The methodology considered herein, based on classical foundations, may provide the above advantages in diverse engineering areas. It exhibits, as main common features, the stages listed in what follows.

(1) The experimental equipment may include diverse instruments now available on the market and it has to be carefully selected. Such selection and the design of

the test procedure at present may or should be based on computer simulations as specified below at point (5).

(2) After the choice of material constitutive models, computer simulations of the test, usually by finite element (FE) methods, are designed with quantification of their accuracy. Specifically, "geometrical nonlinearities" (large strains) and material nonlinearities (elastoplastic models possibly supplemented by fracture and/or time dependence models) are needed in the procedures to be considered here.

(3) Parameters to identify are selected within the constitutive model chosen at the preceding stage and/or they concern stresses due to loads or self-stresses.

(4) Definition of a "search domain" in the space of sought parameters should be specified (by an "expert") on the basis of preceding expertise in the technical context, usually by means of a lower and upper bound for each parameter (and sometimes, if possible, also correlations among sought parameters may be useful to exploit).

(5) For the selection of the quantities to measure, sensitivity analyses are preliminarily performed in order to quantify the influence of each sought parameter on measurable quantities in the response to external actions of the specimen or structure to be tested [Kleiber *et al.* (1997)]. Sensitivity is computed as derivative (suitably approximated by finite difference) of the relationship, established by test simulation, between each measurable quantity and each parameter to estimate. Another computational effort useful for the test design consists in assessing the interval between measurable quantity values computed at conjectured lower and upper bound of each parameter (with other parameters set at their reference mean values). In fact such interval has, clearly, to be much larger (say two orders of magnitude) than the experimental error (say standard deviation) expected from the selected instrument.

(6) Over the "search domain", defined at stage (d), a grid of M "nodes" is adopted, usually by subdividing into equal parts the conjectured variation interval for each parameter. Sometimes the "Latin hypercube sampling" procedure (see e.g., [McKay *et al.* (1979)]) can be preferable in order to limit the number M of "nodes", which otherwise increases exponentially with the search domain dimensionality.

(7) By attributing to the parameters the values corresponding to each grid node, say vector $\mathbf{p}_i$ ($i = 1, \ldots, M$), test simulations are performed leading to vectors $\mathbf{u}_i$ ("snapshots"), each one containing the resulting N measurable quantities.

(8) The computed "snapshots" $\mathbf{u}_i$ usually turn out to be "correlated", as expected due to physical reasons, i.e., they are "almost parallel" vectors in their N-dimensional space. Such circumstance suggests "proper orthogonal decomposition" (POD) and subsequent "model reduction", namely: generation in the snapshot space of a new reference system with axes which maximize norms of the snapshots projections on them; "truncation" of axes with that norm below a certain threshold. The determination of such "new basis"

requires once-for-all computation of the eigenvalues and eigenvectors of matrix $\mathbf{D} = \mathbf{U}^T\mathbf{U}$, where $N \times M$ matrix $\mathbf{U}$ gathers all the M computed snapshots. When the new "basis" is available, the test simulation based on any new parameter vector $\mathbf{p}$ within the search domain can be performed by interpolation through radial basis functions (RBF) among the reduced "amplitudes" of the original snapshots $\mathbf{u}_i$. Such test simulations, which can be carrried out with controllable good approximation, require computing times orders-of-magnitude shorter than further FE analyses of tests. The above POD + RBF procedure is outlined by the flow-chart of Fig. 1, with details in mechanics-oriented literature, see e.g., [Liang *et al.* (2002); Buljak (2011)].

(9) Inverse analysis is here centered on the minimization, with respect to the parameters in vector $\mathbf{p}$, of a "discrepancy function" $\omega(\mathbf{p})$

$$\hat{\omega}(\hat{\mathbf{p}}) = \min_{\mathbf{p}}\{\omega(\mathbf{p})\}, \quad \omega(\mathbf{p}) = [\mathbf{u}_e - \mathbf{u}(\mathbf{p})]\mathbf{C}^{-1}[\mathbf{u}_e - \mathbf{u}(\mathbf{p})], \tag{1}$$

where $\mathbf{u}_e$ is the vector of experimental data and $\mathbf{C}$ represents the covariance matrix of the measurements (intended merely to confer "more weight" to more accurate measurements in the present deterministic approaches).

(10) Procedures for the numerical solution of problem (1) must be selected taking into account possible ill-posedness and nonconvexity of objective function ω and suitable remedies (Tikhonov regularization, multiple initializations). In the research referred to herein the following methods have been employed

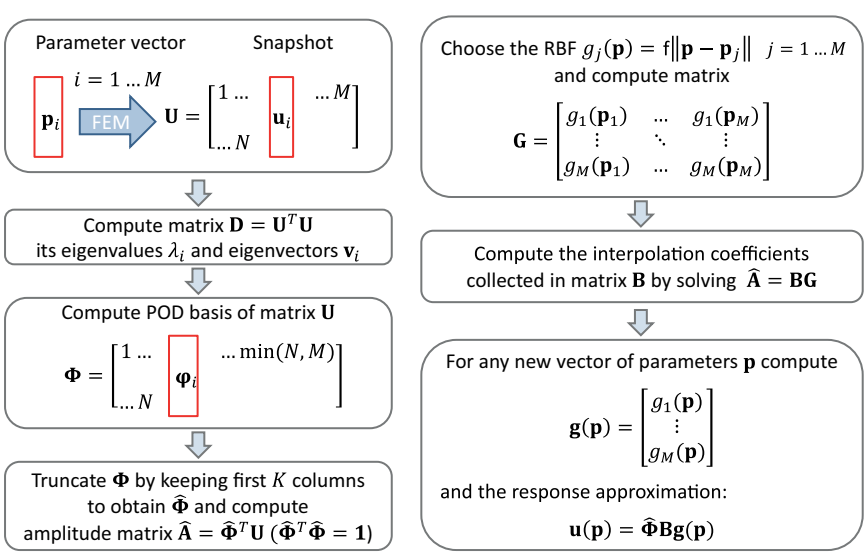

(a) (b)

Fig. 1. Flow-chart of: (a) the POD "model reduction" procedure; (b) RBF interpolations for computation of measurable quantities $\mathbf{u}$ with "new" parameters $\mathbf{p}$.

(sometimes comparatively): "trust region algorithms" (TRA), namely step-by-step mathematical programming based on first-order derivatives; artificial neural networks (ANN); genetic algorithms (GA). No details on these computational methods will be given in what follows; a growing literature and collections of relevant software are at present available, e.g., [Conn *et al.* (2000); Waszczyszyn (1999); Koh and Perry (2009)]. In all investigations carried out so far, the preparatory computational effort related to POD and its repetitive exploitation within the above algorithms turned out to be practically very advantageous.

(11) In view of routine industrial applications, numerical exercises have to be systematically performed in order to comparatively check the inverse analysis procedures adopted. Specifically, for procedure optimization and validation: chosen parameters $\bar{\mathbf{p}}$ are input into direct analysis leading to "pseudo-experimental" measurable quantities $\bar{\mathbf{u}}$, which are employed as input of inverse analysis, the results of which are compared to the original vector $\bar{\mathbf{p}}$.

3. Diagnosis of Metal Structures Based on Indentation Tests

3.1. *Identification of elasticity and plasticity parameters*

Traditional indentation tests originally devised for the assessment of "hardness", since several years have been developed into a nondestructive technique for the calibration of material constitutive models either by semi-empirical formulae (see e.g., [Oliver and Pharr (1992)]), or, later, by test simulations and inverse analyses (see e.g., [Dao *et al.* (2001); Kucharski and Mroz (2004)]).

The use of imprint geometry as an additional source of experimental data for parameter identification has been proposed in [Bolzon *et al.* (2004)]. At present, the following alternative procedures based on indentation can be adopted for diagnosis of structures and plant components (see e.g., [Bocciarelli and Maier (2007); Bolzon *et al.* (2008); Buljak and Maier (2011)]): (A) an instrumented indentation device is employed "*in situ*" to generate loading–unloading curves (Fig. 2(a)) and to transfer them in digitalized form to a computer for inverse analysis; (B) a laser profilometer provides further data on the imprint geometry, Fig. 2(b), to be exploited together with those gathered from the indentation plots; (C) a noninstrumented indenter is employed and only the imprint profiles are used as input for the inverse analysis computations. Procedures (B) and (C) can be carried out either by a profilometer employed "*in situ*", or a suitable replica (e.g., by silicon or polymeric material) can be transferred to a desktop profilometer in a laboratory.

The pseudo-experimental indentation results shown in Fig. 2 (with data for inverse analysis marked by dots) have been achieved in [Bolzon *et al.* (2011)] by the FE commercial computer code Abaqus [SIMULIA, Dassault Systemes] with the following assumptions: diamond indenter sphero-conical with 120° cone opening angle and a 200 μm radius of spherical tip, like in traditional Rockwell tests; classical Ramberg–Osgood material model of isotropic associative hardening

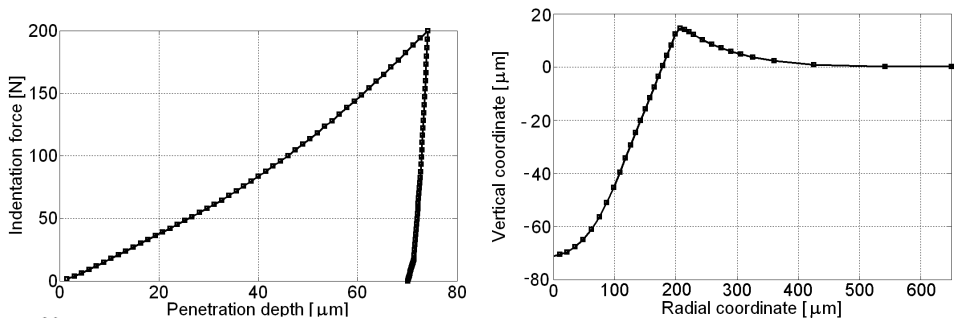

(a) (b)

Fig. 2. (a) Indentation curve and (b) imprint profile.

elasto-plasticity (see e.g., [Jirasek and Bazant (2001)]) with the following parameters: Young modulus $E = 200\,\mathrm{GPa}$, Poisson ratio $\nu = 0.3$, yield stress $\sigma_Y = 380\,\mathrm{MPa}$, hardening exponent $n = 0.092$; friction at the interface with coefficient 0.15 and no dilatancy (therefore "nonassociativity" in terms of plasticity models).

In this numerical exercise, the parameters to estimate are E, σ_Y and n; the inverse analysis procedure POD + ANN is adopted; $M = 5740$ nodes are selected over the "search domain" in the three-dimensional parameter space; the corresponding FE simulations performed according to the POD strategy lead to $N_A = 100$, $N_C = 36$, $N_B = N_A + N_C = 136$ experimental data (visualized in Fig. 2) for approach (A), (C) and (B), respectively. After "truncation" by the same criterion, the "amplitude" vectors $\mathbf{a}_i$ have dimensions 5, 4 and 7, respectively. These are employed as ANN inputs, since they are representative of experimental data as for their meaningful contents. The 5740 available "patterns" have been employed for the ANN training and validation as follows: 50% to compute "weights" and "biases" in all neurons by a Levenberg–Marquardt algorithm; 10% for the ANN optimization reduced to selection of the neuron number in one "hidden" layer only; 40% for "testing" computations apt to check the "generalization" ability of the trained ANN. The number H of neurons in the hidden layer was optimized by minimizing the mean-square error emerging from the validation patterns for different H (here from 2 to 30 neurons).

The above procedures are well established in the literature on soft-computing, see e.g., reference [Waszczyszyn (1999)]. Random perturbations ("noises") with a uniform probability density function in the interval of $\pm 3N$ for the indentation curves and $\pm 3\,\mu$m for the residual imprint, have been added to the pseudo-experimental data before using them as inverse analysis inputs. Figure 3 visualizes in percentage the perturbation consequences on the resulting estimates. The imprint geometry turns out to be more useful than the indentation curve for the identification of the plasticity parameters, and almost as effective as both sources employed together. Experimental noise has its largest influence on the estimation

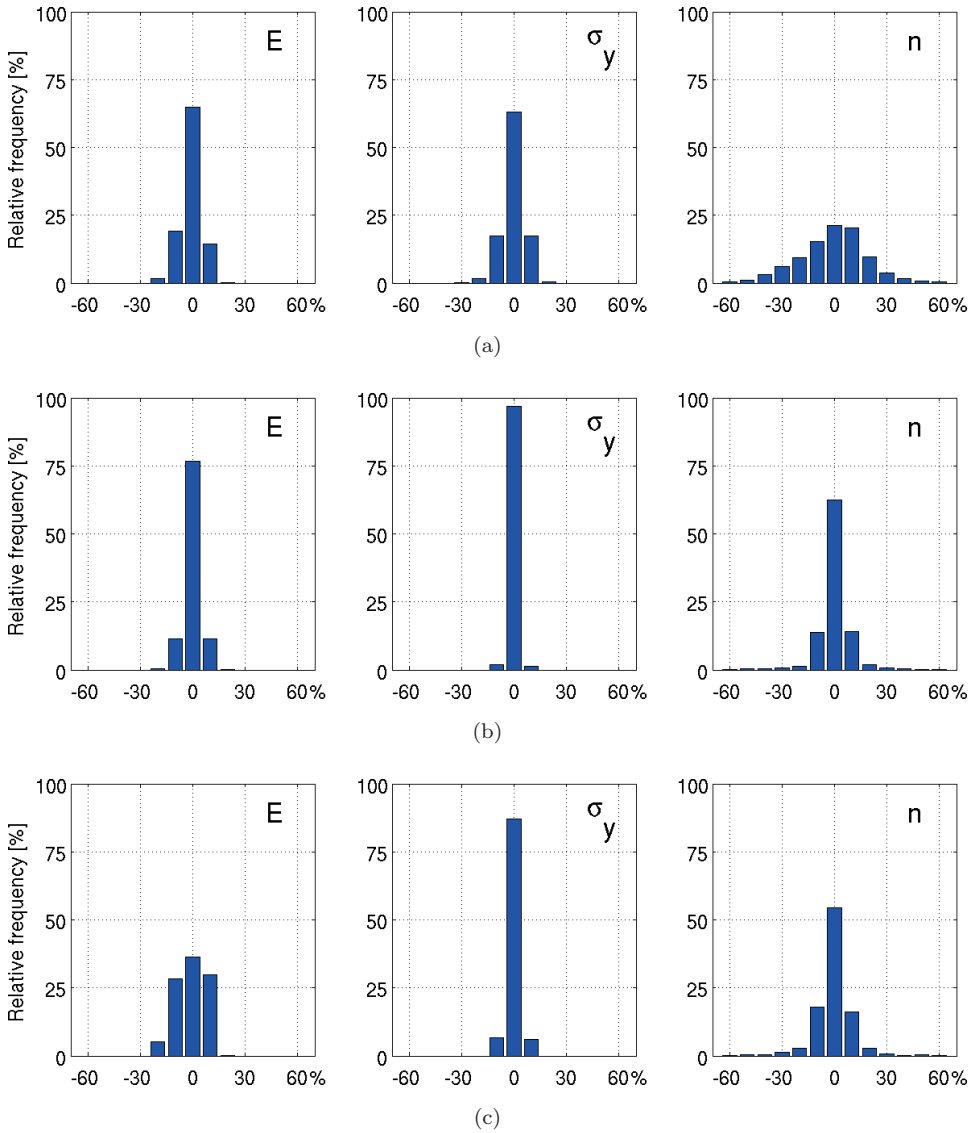

Fig. 3. Distributions of estimates perturbations consequent to the introduction of "noise" in pseudo-experimental data: (a)–(c) are the results for parameter calibration carried out by procedure (A), (B) and (C), respectively.

of Young modulus E when only profilometric measurements are employed according to approach (C). Computational exercises have evidenced the feasibility of the approach (C), its competitiveness with (B) and its preferability with respect to the traditional one (A) when plastic parameters are sought. For many real-life engineering applications of nondestructive indentation testing the following potential

advantages are exhibited by the novel approach (C): available hardness tester can be employed instead of instrumented indenter; practically no influence of supports for load contrast on measurements; applicability to dynamical indentation.

3.2. *Estimation of residual stresses*

Indentation curves generated by the traditional axisymmetric indenters or by indenters with multiple symmetries (pyramidal) cannot provide experimental data apt to completely estimate quantities which change with the orientation. Tensorial quantities important in many engineering situations are employed by anisotropic material models and residual stresses in superficial plane states, due to metal forming or welding processes. The employment of profilometers besides indenters, as proposed in [Bolzon *et al.* (2004)], obviously implies additional costs and becomes practically impossible or difficult in situations like diagnosis of offshore plants under sea level. Therefore indentation-based parameter assessments have been investigated (and presented in [Buljak and Maier (2012)]) with the following features: (a) indenter tips with elliptical (instead of circular) cross-section derived from the traditional conical or spherical indenters; (b) three repeated indentation tests at the vertices of an equilateral triangle, with side length of one or two orders of magnitude larger than the imprint depth; (c) indenter rotations by 45° and 90° degrees in moving from the first to second and third indentation test.

A traditional spherical Brinell-type indenter with diameter D_s is considered in what follows. If the coordinate x along the indenter axis has its origin on the indenter tip, the two diameters of the ellipse generated as new cross-section by shape modification (Fig. 4(a)) can be described by the following formulae:

$$D_{\max} = \beta D_0(x), \quad D_{\min} = (1/\beta) D_0(x), \quad D_0(x) = 2(D_s\, x - x^2)^{1/2}, \tag{2}$$

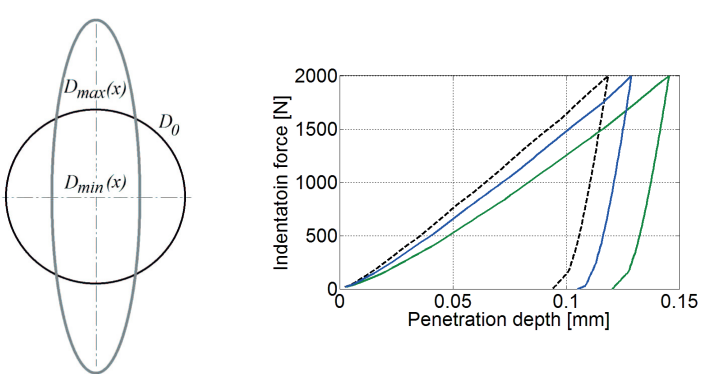

(a) (b)

Fig. 4. Generation of ellipsoidal indenter from a spherical one; indentation curves provided by three tests rotated by 45° one from the other.

where $\beta > 1$ governs the sharpness of the new shape. For preliminary computational exercises the classical isotropic elastic-perfectly-plastic "associative" Huber-Mises model has been adopted in [Buljak and Maier (2012)]. The reference values which quantify the principal residual stress state to identify are $\sigma_I = 500$ MPa, $\sigma_{II} = -500$ MPa, $\varphi = 20°$ being the angle between axis 1 and direction of σ_I. The indenter which turned out to be preferable in comparative computations is ellipsoidal with shape defined by $D_0 = 0.5$ mm and $\beta = 2$; its geometry is specified in Fig. 4(a). Figure 4(b) visualizes the influence on indentation curves of this indenter when indentations are performed three times by rotating it 45° each time. When residual stresses to be estimated exhibit principal directions known *a priori*, a third indentation (at 45°) is useless in view of the small sensitivities of its experimental data. The POD procedure was started by adopting in the parameter space a regular grid with 125 nodes by varying the three parameters within the following ranges: $-600 < \sigma_I < 600$ MPa, $-600 < \sigma_{II} < 600$ MPa; $0 < \varphi < 90°$. Figure 5 visualizes the TRA step sequences up to convergence of discrepancy function minimization. The same optimization procedure was repeated three additional times starting from different initialization vectors. The averages resulting from all the inverse analyses exhibit the following values $\sigma_I = 503$ MPa, $\sigma_{II} = -499$ MPa and $\varphi = 21.9°$. These values turn out to be satisfactory if compared to their counterparts earlier assumed as "targets" (500 MPa, −500 MPa and 20°, respectively).

The study outlined in what precedes has led to the conclusions which follow. The identification of tensorial properties, such as residual stresses, by means of indentation curves alone becomes possible by adoption of indenter with elliptical cross-section and by three indentations carried out near the investigated location in the structural component subjected to diagnostic analyses. After POD and model reduction (Fig. 1(a)), RBF interpolations (Fig. 1(b)) may replace repeated test simulations by FE direct analysis, so that the discrepancy minimization by TRA (see e.g., [Conn *et al.* (2000)]) can be done on site, in a fast, economical fashion using a small portable computer. In fact, the computing time here required by FE simulation turns out to be four orders-of-magnitude larger than the time necessary

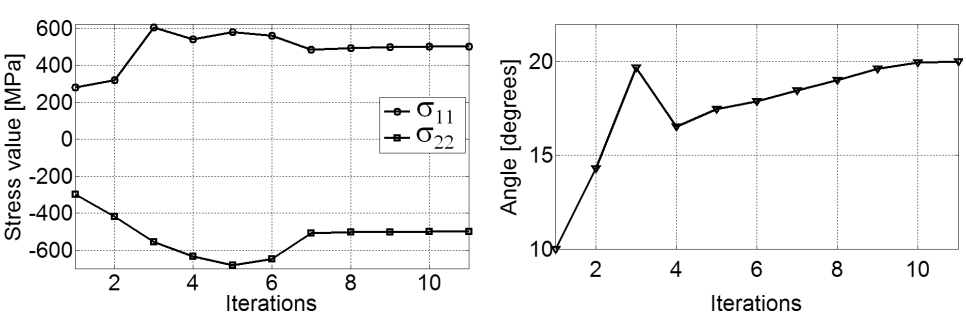

Fig. 5. Sequence of steps of a TRA procedure applied to the estimation of the three parameters which define a residual stress state.

for generating the same "snapshots" of measurable quantities by the POD + RBF procedure. Developments in progress concern the use of a generalized, but conceptually and methodologically similar, procedure for the mechanical characterization of anisotropic materials (also their fracture models), again on the basis of indentation curves alone.

4. Mechanical Characterization of Free Foils and Membranes

4.1. *Parameter identification based on tensile cruciform tests and full-field measurements*

At present thin structural components, subjected in service primarily to stress states in their plane, have an important or even central role in growing industrial fields concerning the following quite diverse products: (i) multilayer laminates for beverage/food containers; (ii) membranes for tension structures in architecture; (iii) coated textiles for a variety of purposes (e.g., sails, airships).

Recent and in-progress research contributions by our team concern field (i) and are partly developed in collaboration with Tetrapak company; however some fall-outs are likely to be useful in the other areas.

The foils employed for beverage/food packages generally exhibit the following features: layers of diverse materials (paper, aluminum, polymers); significant anisotropy due to production process, specifically orthotropy with known principal directions ("machine direction" MD, "cross direction" CD, thickness direction ZD); thickness usually of less than 1 mm; need for local folds generated by creasing. An accurate mechanical model of the laminate is required for the structural design of containers, particularly in view of severe loadings during transportation, but cannot be represented by homogenization since adhesion between sheets may have unpredictable influence on the laminate overall behavior.

An investigation on foil modeling to the above purposes is described with details in [Garbowski *et al.* (2012)] and briefly outlined here below. The following

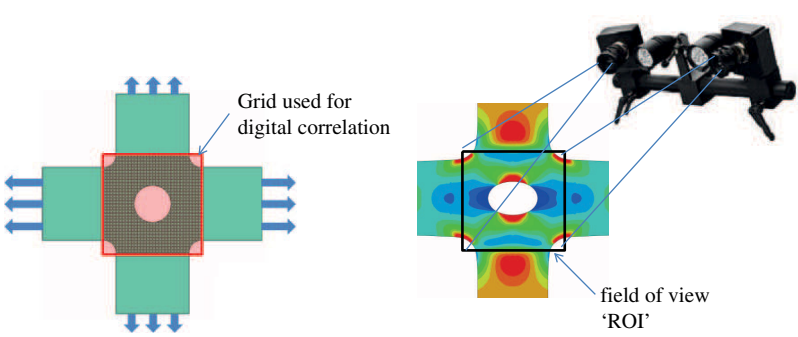

Fig. 6. (a) Cruciform-shape specimen with a hole and (b) schematic DIC system.

experimental provisions are adopted (Fig. 6): cruciform biaxial test with imposed elongations of branches and measurements of consequent forces at the clamps; full-field measurement of two-components displacements by digital image correlation (DIC) techniques (see e.g., [Hild and Roux (2006); Avril *et al.* (2008)]) over a central area ("region of interest", ROI) of the specimen; strain field made strongly nonuniform (but with double symmetry) by a hole in the specimen center.

The elastic–plastic associative, hardening constitutive model here considered for calibration reads:

$$\begin{Bmatrix} \varepsilon_{11} \\ \varepsilon_{22} \\ 2\varepsilon_{12} \end{Bmatrix} = \begin{bmatrix} 1/E_1 & -\nu_{21}/E_2 & 0 \\ -\nu_{12}/E_1 & 1/E_2 & 0 \\ 0 & 0 & 1/G_{12} \end{bmatrix} \begin{Bmatrix} \sigma_{11} \\ \sigma_{22} \\ \sigma_{12} \end{Bmatrix}, \tag{3}$$

$$\dot{\varepsilon}^p = \dot{\lambda}\frac{\partial f}{\partial \sigma}, \quad \dot{\lambda} \geq 0, \quad f\dot{\lambda} = 0, \tag{4}$$

$$f(\sigma, \tilde{\varepsilon}^p, \mathbf{N}_\alpha) = \sum_{\alpha=1}^{6} \left[\chi_\alpha \frac{\mathbf{N}_\alpha^T \sigma}{\sigma_\alpha(\tilde{\varepsilon}^p)}\right]^{2k} - 1 \leq 0, \tag{5}$$

$$\tilde{\varepsilon}^p = (\varepsilon_p^T \varepsilon_p)^{\frac{1}{2}}, \tag{6}$$

$$\chi_\alpha = \begin{cases} 1 & \text{if } \mathbf{N}_\alpha^T \sigma > 0 \\ 0 & \text{if } \mathbf{N}_\alpha^T \sigma \leq 0 \end{cases}, \tag{7}$$

$$\sigma_\alpha = q_\alpha(\varepsilon_0 + \tilde{\varepsilon}^p)^{n_\alpha}, \tag{8}$$

where reference axes x_1, x_2, x_3 are in the orthotropy directions MD, CD, ZD, respectively; classical Hooke law of linear elasticity is expressed by Eq. (1); $\sigma = [\sigma_{11}, \sigma_{22}, \sigma_{12}]^T$, $\varepsilon^p = [\varepsilon_{11}^p, \varepsilon_{22}^p, 2\varepsilon_{12}^p]^T$ represent the stress and plastic strain tensors; unit vectors $\mathbf{N}_\alpha = [N_{11}, N_{22}, N_{12}]_\alpha^T$ define, through orthogonality, six plane "subsurfaces" ($\alpha = 1, \ldots, 6$) which enter into the yield surface definition, with the assumptions: $\mathbf{N}_3 = [0, 0, 1]^T$, $\mathbf{N}_6 = [0, 0, -1]^T$, $\mathbf{N}_4 = -\mathbf{N}_1 = -[\cos\theta_1, \sin\theta_1, 0]^T$, $\mathbf{N}_5 = -\mathbf{N}_2 = -[\cos\theta_2, \sin\theta_2, 0]^T$, θ_1 being the angle between versor $\mathbf{N}_1$ and axis x_1; parameter k governs the "corner smoothing"; χ_α are "switching control" coefficients; $\tilde{\varepsilon}^p$ is the equivalent plastic strain; factor q_α and exponent n_α define the hardening law, ε_0 being a constant to be chosen once-for-all, here $\varepsilon_0 = 10^{-6}$.

The above model, visualized in Fig. 7, has been proposed in [Garbowski *et al.* (2012)] as a slight simplification of the model elaborated for paper and paperboard foils at MIT by Xia, Boyce and Parks (XBP) [Xia *et al.* (2002)]. Such simplification does not reduce significantly the description capacity of the material model (comparisons presented in [Garbowski *et al.* (2012)]) but it reduces from 27 to 17 the number of parameters. These parameters are: Young moduli E_1, E_2, G_{12}, Poisson ratio ν_{12}, parameter k, hardening parameters q_α and n_α ($\alpha = 1, \ldots, 5$), plastic strain ratios $T_1 = \tan\theta_1$ and $T_2 = \tan\theta_2$, for loading in MD and CD directions.

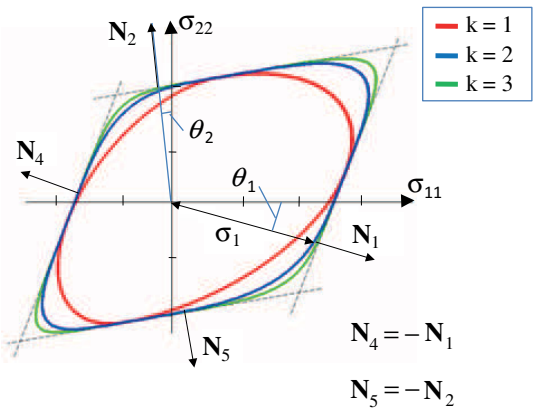

Fig. 7. A plasticity model for paper: intersection of the yield surface with the plane $\sigma_{12} = 0$ (no shear stress) for different values of parameter k.

In the numerical exercises carried out so far, 10 are the loading stages for measurements, at equal increments of the clamp displacements; 241 is the number of grid nodes (and FE mesh nodes) where displacement components, in the foil plane, are measured by DIC; additional experimental data concern the two reactive clamp forces (in MD and CD direction) at the ends of the specimen arms. The FE simulations of cruciform tests performed so far, exploiting the double symmetry, involve 5226 degrees-of-freedom in the specimen plane [Garbowski *et al.* (2012)].

The above chosen sets of measurable quantities, say vector $\mathbf{u}$, are connected by test simulations ("direct analyses") to the above specified vector $\mathbf{p}$ of the 17 material parameters. Among diverse useful sensitivity analyses, two orientative ones led to the plots of Fig. 8 which visualize derivatives of the Euclidean norm of vector $\mathbf{u}$ with respect to each parameter in $\mathbf{p}$. Reasonably expected "reference" values are attributed to components of $\mathbf{p}$ and the increment of 1% in the argument has been adopted for derivative approximations.

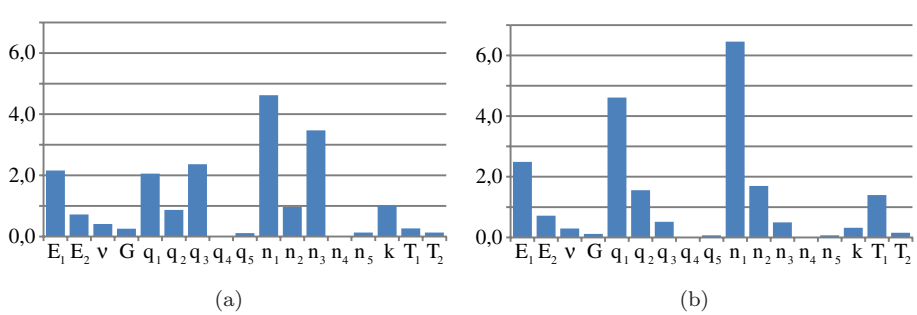

Fig. 8. Sensitivities of measurable quantity norms with respect to the parameters, in biaxial cruciform tests: (a) sensitivities of the displacements measurable by DIC; (b) sensitivities of the reactive forces at the clamps.

Results on sensitivities like those of Fig. 8 show that both kinds of experimental results (DIC displacements and reactive forces) are worth being considered to model calibration purposes and that, as expected, parameters related to foil behaviour under compression (namely q_α and n_α with $\alpha = 4, 5$) cannot be identified by a tension test even if biaxial. Some of the inverse analyses by TRA intended to check identifiability of parameters, comparatively in the original and in the simplified XBP model, are presented in [Garbowski *et al.* (2012)]. With reference to an identification exercise involving 12 out of the 17 parameters of the simplified XBP model (i.e., assuming that ν_{12} is given and that $q_4 = q_1$, $n_4 = n_1$, $q_5 = q_2$ and $n_5 = n_2$), Figure 9 provides the convergence curves obtained by TRA and shows that it is beneficial to exploit as data for the inverse analysis both the displacements in the ROI and the reactive forces at the clamps.

In view of routine applications in an industrial environment, "feed-forward" ANNs have been considered in [Garbowski *et al.* (2011)] as a sequel of the study outlined in what precedes. Generally, for the design and the computational behavior of ANN a balance is desirable between the dimensionalities of vectors **p** and **u**. In the present context the number of experimental data, i.e., the dimensionality of vector **u** containing displacement measurements by DIC, turns out to be by orders of magnitude larger than the dimension of the parameter vector **p**. Therefore the role of ANN input is attributed here again, like in Sec. 3, to "amplitude" vector **a** which approximates the information contained in the snapshot **u** by compressing it through the POD procedure employed in the preceding section. The role of vector **a** is twofold: the preliminary generation of the ANN by means of the "patterns" ($\mathbf{p}_i$, $\mathbf{a}_i$); the input of the ANN for the estimation of the parameters **p** on the basis of a test on cruciform specimen with DIC measurements.

Training, testing and validation here have employed 70%, 15% and 15%, respectively, of the POD pre-computed "patterns". Poisson ratio ν_{12} and the parameters

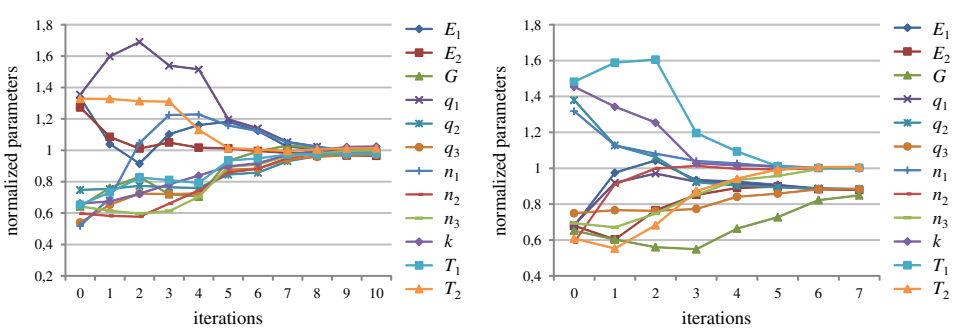

(a) (b)

Fig. 9. Convergence of the inverse analyses performed on the basis of a cruciform biaxial test, using a trust region algorithm (TRA): (a) exploiting both the displacement measurements and the reactive force measurements; (b) exploiting only the measurements of displacements.

governing the compression subsurfaces (q_α, n_α with $\alpha = 4, 5$) have been assumed as given "*a priori*" since the biaxial tension test does not lend itself to the calibration of such parameters, as indicated by the low values of the corresponding sensitivities highlighted in Fig. 8. Over the 12-dimensional "search domain", $M = 10{,}000$ nodes have been generated. At each loading stage the number of experimental data was 484: forces in direction MD and CD; displacements at each one of the grid nodes over the ROI adopted for DIC measurements. The snapshot matrix $\mathbf{U}$ on which the POD procedure is based turns out to have the dimensions $4840 \times 10{,}000$; the POD truncation has been carried out at the 36^{th} eigenvalue of matrix $\mathbf{D} = \mathbf{U}^T\mathbf{U}$. The ANN "architecture" has been designed with a single "hidden layer" containing neurons active with a linear combination and a sigmoidal transformation as usual. Neural networks with different number of neurons in the input layer (due to different level of POD truncation) and with different number of neurons in the hidden layer, were trained and tested. The resulting "best architecture" consists of 36-72-12 neurons in input, hidden and output layer, respectively. With $M = 10{,}000$ training patterns the error mean values of the parameter estimates obtained by the above ANN turn out to be the following ones, in percent: $E_1 = 1.4$; $E_2 = 1.5$; $G = 1.6$; $q_1 = 4.8$; $q_2 = 4.4$; $q_3 = 17.0$; $n_1 = 4.4$; $n_2 = 5.5$; $n_3 = 16.7$; $2k = 9.1$; $T_1 = 4.3$; $T_2 = 4.0$. Error here means distance from the parameter vector $\mathbf{p}_i$ originally used for the ANN training as part of the i^{th} "pattern" to the vector generated by the trained ANN. An obvious difficulty intrinsic to the POD + ANN method is that the growth of the parameter space dimensionality would imply a corresponding exponential growth of the number of grid nodes over the search domain. With reasonable snapshot number in the preliminary POD computations (like 10,000 in the present exercises), the density of nodes over the search domain becomes low and this can jeopardize the accuracy of the estimates provided by the trained ANN. However, as already underlined in the preceding sections, the increase of snapshot number M concerns only the preparatory computations to be done once-for-all and, hence, is quite possible in real-life applications.

4.2. *Parameter estimation based on compression and bending tests*

The mechanical characterization of free foils by experiments with compression in their planes is required by the following circumstances: walls of food containers are often significantly compressed during transportation; anisotropic constitutive models like the ones considered in what precedes involve parameters which cannot be identified by tests with dominant tension. The novel experimental equipment ("sandwich system"), proposed and computationally investigated in [Cocchetti *et al.* (2012)], is schematically shown in Fig. 10. A rectangular specimen of the foil is inserted between two stabilizing elastic "blocks". The external actions consist of rotations imposed by two rigid clamps, apt to generate a chosen combination of compression and bending. At each step of the planned rotations, many displacements are measured by the DIC technique, both on the blocks and on the emerging

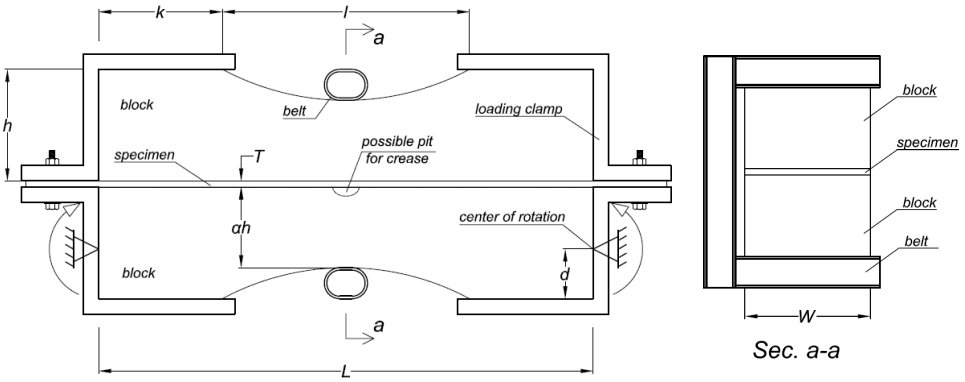

Fig. 10. "Sandwich system" for compression-bending tests.

specimen. FE computer simulations are performed, first for sensitivity analyses apt to design and optimize the procedure; subsequently the POD + RBF + TRA procedure is applied to the estimation of parameters. A "fictitious homogeneous material" is attributed to the foil (even if it is a layered laminate) and its behavior is described by an anisotropic elastic–plastic model (Hill model for the first validation exercises in [Cocchetti *et al.* (2012)]). Homogeneity assumption is suggested by unpredictable changes in local properties of layers and interfaces due to the production processes. Subsequently, a fast transition to generalized variables is performed by adopting a traditional elastic–plastic "beam model" with isotropic hardening. The present parameter estimation in these two phases is suggested by limitations of some popular FE commercial codes like the one employed in this study and in the related industry.

Figure 11(a) visualizes the simple model here adopted in generalized variables (per unit transversal width of the specimen), namely axial force N (compression

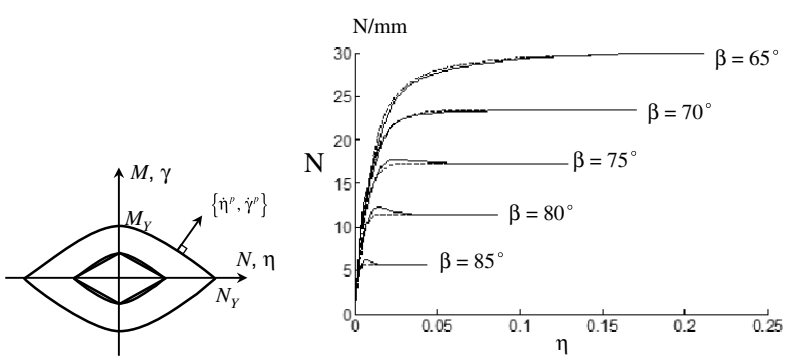

(a) (b)

Fig. 11. Generalized variables model (a); comparison between axial behaviors of foil specimen resulting from two assessments of the model parameters (b).

positive), bending moment M and relevant generalized strains η and γ. In Fig. 11(b), the specimen axial behavior resulting from the above model calibrated by a second simple parameter identification, based on the earlier calibrated material model, is compared to the behavior resulting from the same material model through classical beam theory. Angle β governs the linear itinerary considered for the deformation process combining compression and bending, namely $\gamma T = \eta \tan \beta$, T being the foil specimen thickness. Further developments in progress concern the design optimization of the novel sandwich geometry for various categories of free-foils employed by the containers industries; the preparatory computations required by POD model reductions have to be performed for each category, but once-for-all again.

5. Assessment of Damages in Concrete Dams

5.1. *Superficial flat-jack tests and inverse analyses*

Structural deteriorations of concrete dams may be caused by: earthquakes, slow motions of the surrounding geological masses, physico-chemical processes, particularly the one called alkali-silica reaction (ASR). Several dams built-up decades ago, particularly in Europe and North America, turn out to be affected by ASR, which, after a dormant period, slowly gives rise to substantial decay of mechanical properties of concrete and to nonuniform expansions with consequent self-equilibrated stresses additional to those due to external actions.

Diagnostic analyses of concrete dams at present can be performed by the following approaches and methods: (a) experiments by flat-jacks on the dam surface; (b) in depth coring or overcoring tests, usually with extraction of specimens for the laboratory; (c) overall dynamical inverse analyses based on excitations by vibrodynes and measurements by accelerometers, see e.g., [Loh and Wu (2000)]; (d) statical overall inverse analyses under loading due to "*ad hoc*" changes of water level in the reservoir, with measurements of consequent displacements by means of pendula, collimators and/or interferometric radar, e.g., [Fedele *et al.* (2006)]; (e) same as (d), but with loading provided by seasonal, in-service variation of reservoir level, e.g., [Ardito *et al.* (2008)].

Diagnostic procedures (c)–(e) are not considered here because they rely on linear-elastic structural responses and, hence, lead only to the assessment of Young modulus distribution. As for structural diagnosis (a) based on flat-jack tests and inverse analysis, the following novelties have been proposed to the engineering practice in [Fedele and Maier (2007); Maier *et al.* (2010); Garbowski *et al.* (2011)]: (i) less destructive geometric configuration of the set of slots; (ii) use of DIC as full-field displacement measurement technique; (iii) assessment of inelastic parameters additional to elasticity and of the existing stress state; (iv) parameter identification performed in a fast and inexpensive fashion (possibly *in situ* by a portable computer) by one of the computational procedures outlined in the preceding sections.

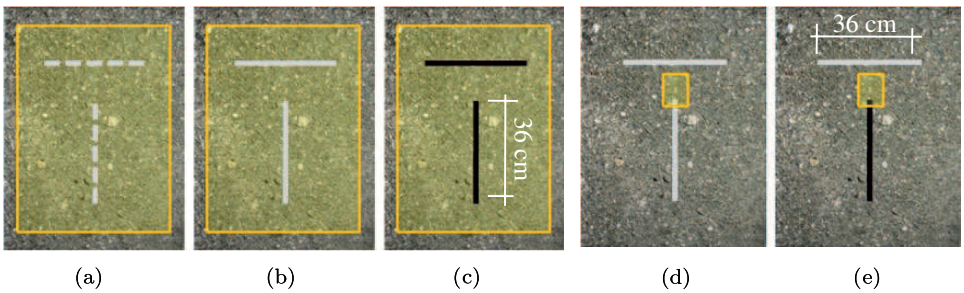

Fig. 12. Sequence of steps in the novel flat-jack tests combined with parameter identification by inverse analysis.

The sequence of operative steps of the proposed diagnostic technique based on flat-jack tests is outlined here below with reference to Fig. 12 (details in [Garbowski *et al.* (2011)]).

(1) In the selected place on the structure surface, the position of two future orthogonal slots (T-shape geometry) is marked and a first photograph is taken over the ROI which is depicted in Fig. 12(a).
(2) The two slots are cut (Fig. 12(b)) and a second photo is shot by the DIC equipment so that the displacements due to the release of the pre-existing stresses in the cut can be measured at all grid nodes.
(3) Two flat-jacks are inserted and pressurized and a DIC photo is taken again in order to capture the new displacement full-field.
(4) The horizontal jack is removed and the vertical one is depressurized. A reference photo is taken of a zone (ROI) located near the upper end of the vertical slot, in which inelastic deformations are expected to develop.
(5) The vertical flat-jack is pressurized in order to generate plastic strains and a quasi-brittle fracturing process near the tips of the loaded slot. A sequence of DIC photos is taken to capture the nonlinear evolution of the displacements due to such pressure loading.

The parameters identifications are performed according to the following sequence of phases: (I) elastic moduli, on the basis of experimental data concerning transition from stage (b) to (c); (II) stresses, on the basis of the elastic moduli estimates achieved in phase (I) and of data acquired at stages (a) and (b); (III) inelastic parameters, on the basis of data concerning the transition from stage (d) to the various deformation stages represented in the sequence of DIC photos taken in phase (e).

The FE model adopted, in [Garbowski *et al.* (2011)] and here, for the computer simulations of the tests includes: 97,600 tetrahedral elements with linear shape functions for displacements and 57,280 degrees of freedom; boundary conditions with

vanishing displacements on the borders separating the domain from the surrounding volume supposed to be not perturbed by the test.

Orthotropy with "transversal" isotropy in the horizontal plane, may be generated in dam concrete by the casting process, especially in roller-compacted concrete. Therefore there are five independent elastic parameters. The identification procedures concern the three parameters which play the main role in the system response, namely horizontal E_{H} and vertical E_{V} Young modulus and the shear stiffness G_{V}. The sought pre-existing stress state can be reasonably assumed to be a plane stress state at the free surface of the dam, uniform over the whole volume affected by the test; hence it is governed by the three components σ_{H}, σ_{V} and τ_{HV} as parameters to identify.

For the plastic behavior of concrete the classical Drucker–Prager model (perfect plasticity with nonassociated flow rule) governed by three parameters, has been adopted in the preliminary validation exercises [Garbowski *et al.* (2011)]. Fracture is supposed to be first-mode only and reducible to a cohesive crack model, in terms of normal stress versus opening displacement, with linear softening [Jirasek and Bazant (2001)].

Computational exercises of parameter identification based on pseudo-experimental DIC data have been carried out in order to validate the proposed

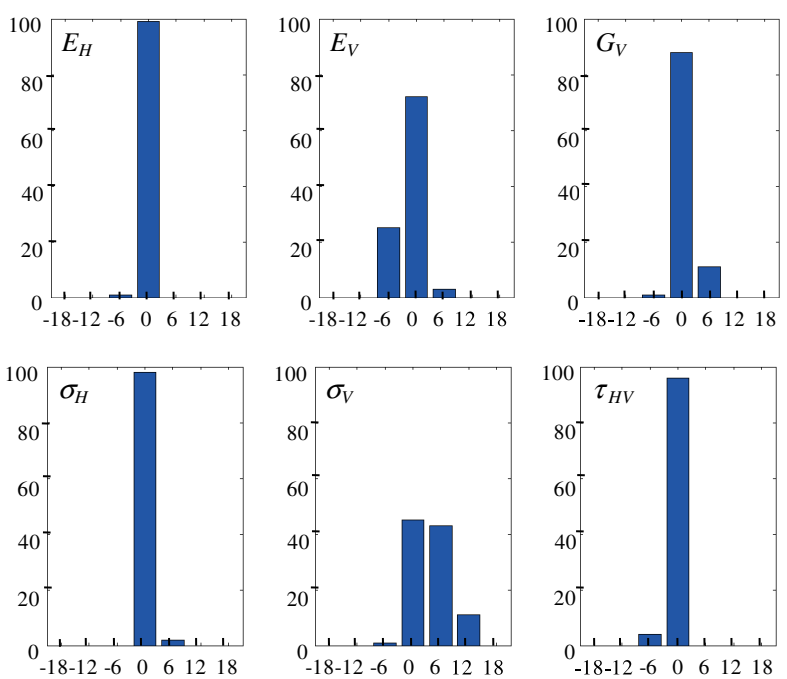

Fig. 13. Results of POD + RBF + TRA procedure for parameter identification based on flat-jack tests: relative errors in the estimates of elastic moduli and initial stresses.

method, comparatively by the three procedures already outlined in the preceding sections: TRA alone; POD + RBF + TRA; POD + ANN. The results achieved and presented in [Garbowski *et al.* (2011)] encourage practical applications. Computationally the second procedure turned out to be slightly preferable. Figure 13 visualizes results achieved starting from pseudo-experimental DIC data perturbed by random noise of $\pm 5\,\mu$m (with uniform probability density over this interval): in absissa intervals of relative errors (in percent), in ordinates percentage of results affected by errors falling within such intervals.

With respect to the present flat-jack practice, the above novel procedure resting on inverse analyses exhibits the following advantages: more information provided, including inelastic parameters; more accurate estimates; less "destructivity" due to simpler slot geometry. Operatively the main difficulty will consist in the design and realization of supports apt to carry the cameras by avoiding disturbances due to the slot drilling.

5.2. *In-depth drilling tests and inverse analyses*

In dam engineering the assessment of possibly deteriorated concrete properties and of the stress state is necessary also in depth, not only near the free surfaces, in order to compute the safety factors with respect to various kinds of failures. The in-depth material characterization is a well developed topic in rock mechanics (see e.g., [Wittke (1990)]). The proposed diagnostic method, developed in [Zirpoli *et al.* (2008)] and schematically illustrated in Fig. 14, can be outlined as follows:

(1) A hole is drilled in the dam.
(2) A device called "dilatometer" is inserted, consisting of two sleeves equipped with radial displacement gouges and, between them, two movable steel "arches".

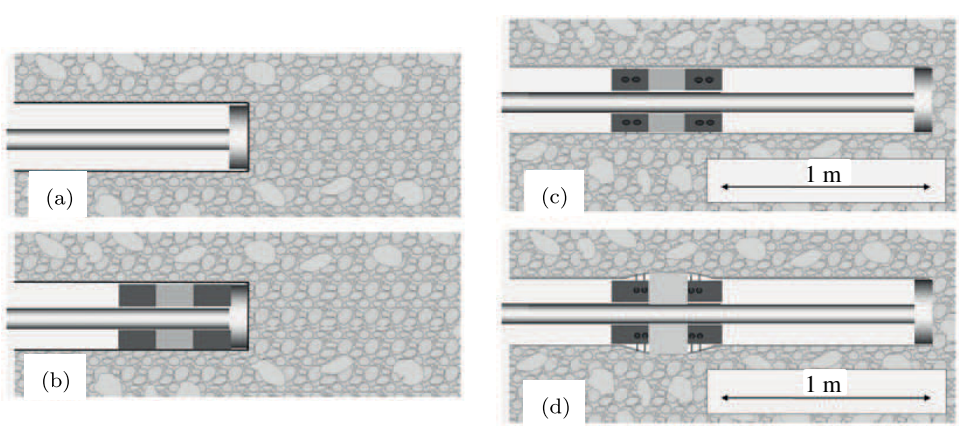

Fig. 14. Operative phases of the proposed procedure based on dilatometric tests.

(3) The drilling goes ahead, while the gouges measure the displacements due to the consequent stress relief.
(4) The two steel "arches", governed by small hydraulic jacks, apply two growing radial forces on the hole wall and the gouges measure the displacements; in this phase a linear elastic response is assumed.
(5) The elastic limit is overcome by increasing the jack pressure.
(6) A portable computer containing an artificial neural network, trained through FE simulations of the mechanical test, on the basis of the displacement data coming from the gouges, performs inverse analyses by the POD + ANN procedure outlined in Secs. 3 and 4. The sought parameters are estimated in the following sequence: Young modulus and Poisson ratio, using the experimental data collected during phase (d); the initial stresses, two normal and one tangential, in the plane orthogonal to the hole axis, by employing data coming from phase (c) and the just estimated elasticity parameters; parameters governing a plastic constitutive model and/or a quasi-brittle fracture model, using measurements in phase (e) and the previous estimates.

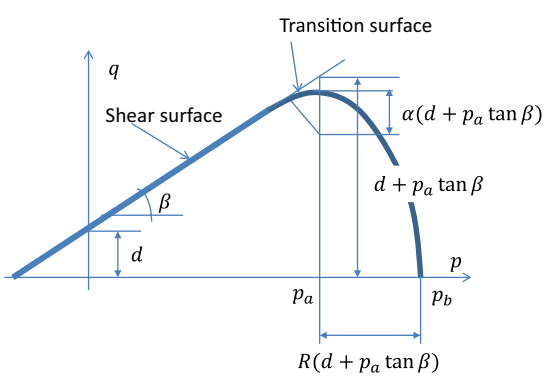

(a)

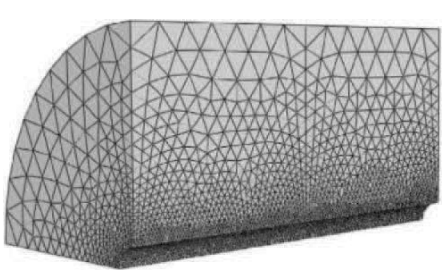

(b)

Fig. 15. Drucker–Prager model with "cap" (a) and FE mesh for one quarter of the problem domain (b).

The above diagnostic procedure is motivated by the following advantages with respect to the state-of-the-art diagnosis inside dams.

(α) No specimen is extracted from the borehole to be tested in laboratory.
(β) Displacements are measured, not strains which are sensitive to local material properties, different from mortar to aggregate.
(γ) Inelastic properties can be assessed "*in situ*" and in depth.

The preliminary computational validation of the method by a pseudo-experimental approach is briefly outlined here below (some details in [Zirpoli *et al.* (2008)]). In the simulations the following simplifying assumptions are adopted:

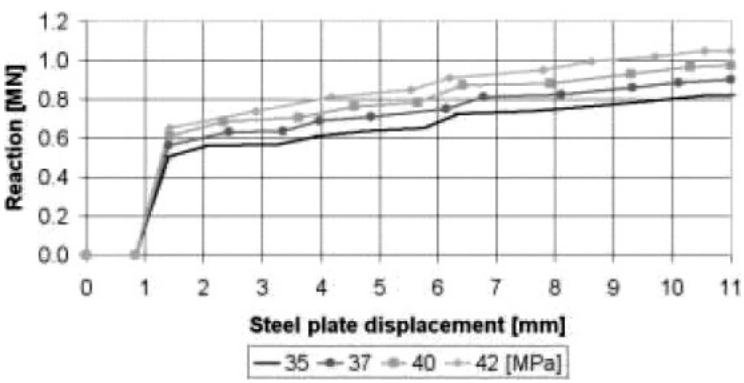

(a)

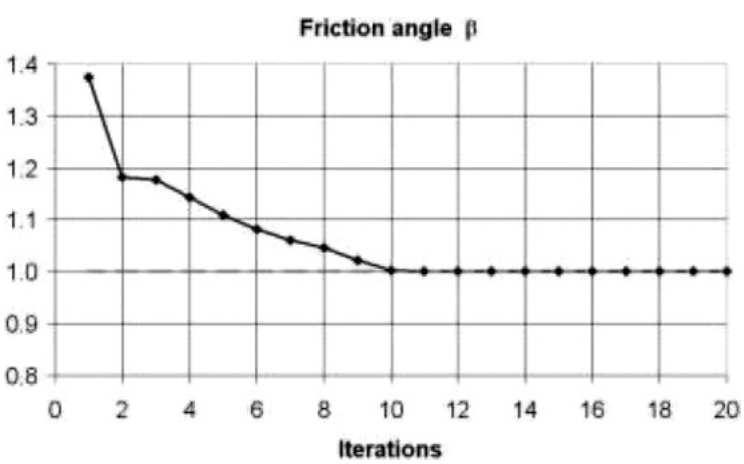

(b)

Fig. 16. Force versus displacement of the "arches" with various values of hydrostatic compressive strength p_b (a); convergence of the TRA identification process as for the normalized internal friction angle β (b).

material isotropy; symmetry of the system with respect to the vertical and horizontal planes through the borehole axis; vanishing displacements on the remote boundary; uniform initial stress field (i.e., before drilling), with vanishing principal stress in the direction of the hole axis; linear elasticity with only Young modulus E to identify; Drucker–Prager model (Fig. 15(a) of perfect plasticity (three parameters to identify: cohesion d, hydrostatic compressive strength p_b and internal friction angle β), improved by a "cap" (one additional parameter: cap eccentricity R) in view of expected stress states with dominant compression.

Figure 15(b) shows the FE model adopted, consisting of about 58,000 linear tetrahedral elements; the analyses were performed by the commercial code Abaqus. Figure 16(a) shows some plots of imposed force versus resulting displacement of the "arches", obtained by attributing different values to the parameter p_b which, together with R, governs the cap. Plots like these visualize the sensitivity of measurable quantities with respect to the sought parameters. A study of such sensitivities can show whether the envisaged measurements are likely to be adequate for the identification of the sought parameters.

The minimization of the usual discrepancy function has been tackled here again by a "trust region" iterative algorithm (TRA). A typical convergence curve for the sought parameters, as iterations proceed, is visualized in Fig. 16(b), which specifically refers to the identification of the internal friction angle β in the model visualized by Fig. 15(a). Such curve is drawn in terms of "normalized" friction angle β/β_0, where β_0 belongs to the set of values (E_0, d_0, β_0, etc.) assumed to generate by direct analyses the pseudo-experimental data (employed as input for the inverse analysis). Further improvements of the present dilatometric methods are now investigated by means of the following provisions: sharp indenters, employed after the arches, apt to provoke fractures, in order to assess fracture properties; generalization of the procedure to poroplasticity and two-phase material models, in order to make it useful to oil and gas industries for drilling techniques.

6. Conclusions

Fruitful associations of computational procedures for back-analysis with experiments have been outlined in what precedes with reference to three quite different engineering problems: diagnosis of metal structures by nondestructive indentation testing (identification of parameters in elastoplastic models and of residual stresses); mechanical characterization of laminated foils, with a paper core layer, for food containers (calibration of anisotropic models both by cruciform tension and novel "sandwich" compression tests); parameter estimation in concrete dams with possible damage diffusion (flat-jack tests near free surfaces, in-depth "dilatometric" experiments).

This survey has been limited to the expertise of our team on real-life problems tackled in collaboration with diverse industries (details in cited recent publications); other restrictions concern the here adopted deterministic approaches and statical

experiments only. Despite the above limitations, it is believed that the practical usefulness of the synergistic combination of computational and experimental mechanics clearly emerges from the present survey. In the three kinds of practical inverse problems considered, the main innovative contributions of industrial relevance have been sensitivity analyses for the design of the experiments, provisions to overcome difficulties arising from possible lack of convexity of the discrepancy function to minimize, and "model reductions" (by "proper orthogonal decomposition") apt to make parameter estimation fast, economical and, in some contexts, performable "*in situ*". Research in progress concerns extensions of the above practical benefits to stochastic approaches and to some dynamical experiments.

Acknowledgments

The authors express congratulations to Professor Nguyen-Dang Hung for his internationally appreciated successes as scientist, research leader and poet as well.

Thanks are addressed to colleagues, both in our university and in various industries, and to visitors and doctoral students in our Department, for valuable contributions to the researches outlined herein.

References

Ardito, R., Maier, G. and Massalongo, G. [2008] "Diagnostic analysis of concrete dams based on seasonal hydrostatic loading," *Eng. Struct.* **30**, 3176–3185.

Avril, S., Bonnet, M., Bretelle, A. and Grediac, M. [2008] "Overview of identification methods of mechanical parameters based on full-field measurements," *Experiment. Mech.* **48**, 381–402.

Bocciarelli, M. and Maier, G. [2007] "Indentation and imprint mapping method for identification of residual stresses," *Comput. Mater. Sci.* **39**, 381–392.

Bolzon, G., Maier, G. and Panico, M. [2004] "Material model calibration by indentation, imprint mapping and inverse analysis," *Int. J. Solids Struct.* **41**, 2957–2975.

Bolzon, G., Bocciarelli, M. and Chiarullo, E. J. [2008] "Mechanical characterization of materials by microindentation and AFM scanning. Identification of residual stresses," in *Appl. Scanning Probe Meth.*, eds. B. Bhushan and H. Fuchs (Springer, Berlin Heidelberg).

Bolzon, G., Buljak, V., Maier, G. and Miller, B. [2011] "Assessment of elastic–plastic material parameters comparatively by three procedures based on indentation test and inverse analysis," *Inverse Problems Sci. Eng.* **19**, 815–837.

Bui, H. D. [1944] *Inverse Problems in the Mechanics of Materials: An Introduction* (CRC Press, Boca Raton, Florida, USA).

Bui, H. D. [2006] *Fracture Mechanics: Inverse Problems and Solutions* (Springer, Berlin Heidelberg).

Buljak, V. [2011] *Inverse Analyses with Model Reduction: Proper Orthogonal Decomposition in Structural Mechanics* (Springer, Berlin Heidelberg).

Buljak, V. and Maier, G. [2011] "Proper orthogonal decomposition and radial basis functions in material characterization based on instrumented indentation," *Eng. Struct.* **33**, 492–501.

Buljak, V. and Maier, G. [2012] "Identification of residual stresses by instrumented elliptical indentation and inverse analysis," *Mech. Res. Commun.* **41**, 21–29.

Cocchetti, G., Mahini, M. R. and Maier, G. [2012] "Mechanical characterization of foils with compression in their planes," *Mechanics of Advanced Materials and Structures*, in print.

Conn, A. R., Gould, N. I. M. and Toint, P. L. [2000] *Trust-Region Methods* (Society for Industrial and Applied Mathematics, Philadelphia, USA).

Dao, N., Chollacoop, N., van Vliet, K. J., Venkatesh, T. A. and Suresh, S. [2001] "Computational modeling of the forward and reverse problems in instrumented sharp indentation," *Acta Materialia* **49**, 3899–3918.

Fedele, R. and Maier, G. [2007] "Flat-jack tests and inverse analysis for the identification of stress states and elastic properties in concrete dams," *Meccanica* **42**, 387–402.

Fedele, R., Maier, G. and Miller, B. [2006] "Health assessment of concrete dams by overall inverse analyses and neural networks," *Int. J. Fracture* **137**, 151–172.

Garbowski, T., Maier, G. and Novati, G. [2011] "Diagnosis of concrete dams by flat jack tests and inverse analyses based on proper orthogonal decomposition," *J. Mech. Mater. Struct.* **6**, 181–202.

Garbowski, T., Maier, G. and Novati, G. [2012] "On calibration of orthotropic elastic–plastic constitutive models for paper foils by biaxial tests and inverse analyses," *Struct. Multidisciplinary Optimiz.* **46**, 111–128.

Hild, F. and Roux, S. [2006] "Digital image correlation: From displacement measurement to identification of elastic properties: A review," *Strain* **42**, 69–80.

Jirasek, M. and Bazant, Z. P. [2001] *Inelastic Analysis of Structures* (Springer, Berlin Heidelberg).

Kleiber, Antunez, H., Hien, T. D. and Kowalczyk, P. [1997] *Parameter Sensitivity in Nonlinear Mechanics. Theory and Finite Element Computations* (John Wiley and Sons, West Sussex, United Kingdom).

Koh, C. G. and Perry, M. J. [2009] *Structural Identification and Damage Detection using Genetic Algorithms* (CRC Press, Boca Raton, Florida, USA).

Kucharski, S. and Mroz, Z. [2004] "Identification of material parameters by means of compliance moduli in spherical indentation test," *Mater. Sci. Eng. A* **379**, 448–456.

Liang, Y. C., Lee, H. P., Lim, S. P., Lin, W. Z., Lee, K. H. and Wu, C. G. [2002] "Proper orthogonal decomposition and applications — Part I: Theory," *J. Sound Vib.* **252**, 527–544.

Loh, C. H. and Wu, T. C. [2000] "System identification of Fei-Tsui arch dam from forced vibration and seismic response data," *J. Earthq. Eng.* **4**, 511–537.

Maier, G., Bolzon, G., Buljak, V., Garbowski, T. and Miller, B. [2010] "Synergistic combinations of computational methods and experiments for structural diagnosis," *Comput. Meth. Mech.* Lectures of the CMM 2009, eds. Kuczma, M. and Wilmanski, K. (Springer-Varlag, Berlin, Heidelberg).

McKay, M. D., Beckman, R. J. and Conover, W. J. [1979] "A comparison of three methods for selecting values of input variables in the analysis of output from a computer code," *Technometrics* **21**, 239–245.

Oliver, W. C. and Pharr, G. M. [1992] "An improved technique for determining hardness and elastic modulus using load and displacement sensing indentation experiments," *J. Mater. Research* **7**, 1564–1583.

Waszczyszyn, Z. [1999] *Neural Networks in the Analysis and Design of Structures* (Springer, Berlin Heidelberg).

Wittke, W. [1990] *Rock Mechanics* (Springer, Berlin Heidelberg).

Xia, Q. S., Boyce, M. C. and Parks, D. M. [2002] "A constitutive model for the anisotropic elastic–plastic deformation of paper and paperboard," *Int. J. Solids Struct.* **39**, 4053–4071.

Zirpoli, A., Maier, G., Novati, G. and Garbowski, T. [2008] "Dilatometric tests combined with computer simulations and parameter identification for in-depth diagnostic analysis of concrete dams," in *Proc. 1st Int. Symp. Life-Cycle Civil Engineering* (*IALCCEE-08*), eds. Biondini, F. and Frangopol, D. M. (CRC Press), pp. 259–264.